Laser Shock Processing of AMg6 Alloy without Coating

I. A. Bakulin[a], *, S. I. Kuznetsov[a], **, A. S. Panin[a], ***, and E. Yu. Tarasova[a], ****

[a] *Lebedev Physical Institute (Samara Branch), Russian Academy of Sciences, Samara, 443011 Russia*
*e-mail: bi205@fian.smr.ru
**e-mail: kuznetsov@fian.smr.ru
***e-mail: anton@fian.smr.ru
****e-mail: kat@fian.smr.ru
Received July 9, 2020; revised October 1, 2020; accepted November 30, 2020

Abstract—The structure and stressed state of AMg6 alloy have been studied after laser shock processing without protective coating. The method of layer-by-layer X-ray structural analysis has revealed a correlation between the parameters of crystalline structure and the profile of residual stresses of the processed samples. After laser processing, the sizes of coherent scattering regions on the material surface decrease to 50 nm, the value of microstrains increases to 0.0019, and the average dislocation density increases to $4.7 \times 10^{14} \text{ m}^{-2}$. The profile and the depth of the residual compressive stresses depend on the power density, coefficient of overlapping of laser spots, and multiplicity of processing, reaching 2 mm.

INTRODUCTION

Investigations in the field of laser shock processing have been actively developing in the last 25 years. This is related to the possibility of its application for processing of engineering materials with the aim of improvement of strength and, in particular, fatigue properties, corrosion, and wear resistance.

In the conventional variant, the essence of laser shock peening is in the action of short laser pulses (10−50 ns) with high power density ($10^9−10^{10}$ W/cm^2) on the surface under processing with a preliminarily applied absorbing coating via a layer transparent to irradiation (water or glass). Under the impact of iradiation in the vapors of the absorbing coating surface, plasma is generated, which forms a shock wave in the material. If pressure in the shock wave exceeds the Hugoniot elastic limit, there occurs plastic deformation of the surface layer of the material under processing and, as a consequence, there occur residual compressive stresses. The absorbing coating, that is, paint, adhesive tape, or foil, in such a processing sequence protects the surface against contact with laser-induced plasma and the transparent layer constrains the plasma from rapid expansion. Contrary to mechanical peening, the front of shock wave upon laser shock treatment is flat, the surface relief after processing changes insignificantly, and the peening depth can achieve 1.5−2 mm. The resistance of products against cyclic loads after such processing can increase from 30 to 200% and even higher [1−4].

In recent years, both conventional methods of laser shock peening (LSP) under the impact of high energy nanosecond pulses with the wavelength of 1.06 μm on a surface with an absorbing layer were developed, and more advanced approaches such as laser shock processing with heating of material under processing [4−6] and laser shock peening without coating (LSPwC) by irradiation of low energy (from units to tenths of joule) with the wavelength of 0.532 μm were developed [7, 8].

In the course of laser processing of surface without coating with the aim of induction of surface plasma, it is required to evaporate a part of material under processing, which is a major drawback of such processing method. However, the absence of absorbing coating is also an advantage, since application of such coatings requires preliminary preparation of the surface, up to polishing, and the shape of products does not always allow coatings to be applied. In addition, lower energy of laser pulses makes it possible to transfer them via optical fiber, and shorter wavelength makes it possible to process items submerged in water to significant depth [9].

The researchers in [10] presented the experimental results of laser shock processing of the structure and residual macro stresses in AMg6 alloy during processing with absorbing coating. Selection of AMg6 as the object of research was dictated by the wide scope of its application in industry, from mechanical engineering to the aerospace field, and the absence of works on

laser shock processing of such alloy; the main method of improvement of strength properties of such alloy is plastic deformation, since AMg6 belongs to alloys which are not hardened by thermal processing.

This work is aimed at studies of the stressed state and structural changes in AMg6 alloy during laser shock processing without absorbing coating.

EXPERIMENTAL

The experiments were carried out on flat samples with the dimensions of $15 \times 15 \times 4$ mm cut out from a sheet of commercial AMg6 polycrystalline alloy with a cladding aluminum layer with thickness up to 70 μm. The composition of the initial samples was in conformity with GOST (State Standard) 4784-97; residual stresses on the surface were absent. Prior to laser processing, the cladding layer in most cases was removed by electrolytic polishing in a solution of hydrochloric acid $HClO_4$ in ethyl alcohol (1 : 4); then the samples were washed with distilled water and acetone.

The pulse source was an LSP 2500 YAG:Nd solid state laser (wavelength $\lambda = 0.532$ μm, pulse duration $\tau = 10$ ns, pulse energy $E = 0.34$ J). Processing of samples without absorbing coating was performed under the running layer of distilled water with the thickness of 60 mm at step-by-step displacement l with overlapping of laser spots. In the course of experiments, the following parameters were varied: the power density $q = 0.1–2.2$ GW/cm^2, the coefficient of overlapping $k_o = (d − l)/d$, the number of processing events (1–3), and the state of surface under processing (existence or absence of protective aluminum layer). The power density was varied by changes in beam diameter $d = 1.4–6$ mm by means of a focusing lens with the focal distance of 100 mm. Upon repeated processing, the sample was rotated by 90° before each subsequent cycle of processing.

Preparation of transverse polished cross sections of processed samples was carried out by their consecutive grinding and polishing on a felt disk wetted with an aqueous suspension of chromium oxide. Then, electrolytic polishing was carried out in a solution of perchloric acid $HClO_4$ in ethyl alcohol for 1–2 min. At final stage, the grain boundaries were revealed by etching with Keller's reagent (10 mL HF, 15 mL HCl, 25 mL HNO_3, 5 mL H_2O).

The microstructure of the considered materials was analyzed using a Neophot 30 optical microscope and an EVO 50 electron microscope (Carl Zeiss) coupled to an INCA Energy 300 spectrometer for elemental analysis. The microhardness of the materials was measured with a PMT-3 hardness meters at the load of 50 g (impression diagonal of 30–40 μm). X-ray structural analysis was carried out using a DRON-3 X-ray diffractometer with CuK_α radiation. The diffraction lines for analysis of structural changes were recorded by points with increment of 0.01°. The X-ray beam was formed using Soller slits, horizontal (0.5 mm) and vertical (6 mm) forming slits, and also a horizontal silt before the counter with the width of 0.2 mm.

The distribution of residual macro stresses across the depth was studied using layer-by-layer removal of material with the increment of 20–150 μm (depending on the processing depth) by electrochemical polishing in solution of perchloric acid $HClO_4$ in ethyl alcohol. Macro stresses in each layer were determined by displacement of the most distant diffraction aluminum line (511) by the $\sin^2\psi$ method (the slope method). The X-ray beam was formed using horizontal and vertical forming slits with the sizes of 2 mm and horizontal silt before the counter with the width of 0.5 mm. Owing to the necessity to obtain numerous experimental data, the diffraction peaks were recorded at two slope angles $\psi = 0$ and $50°$ by points with the increment of 0.02°. The AMg6 sample annealed at 350°C for 2 h was used as the reference. The stresses σ_x and σ_y were determined along and across laser passes, respectively. The stresses were calculated as follows [11]:

$$\sigma_\varphi = \frac{E}{1+\nu} \frac{\varepsilon_{\psi_{50}} - \varepsilon_{\psi_0}}{\sin^2 \psi_{50} - \sin^2 \psi_0},$$

$$\varepsilon = \frac{d - d_0}{d_0},$$

where E is Young's modulus, ν is the Poisson coefficient, ε is the relative change in interplanar distance, d is the interplanar distance (511) of processed samples, and d_0 is the interplanar distance (511) of reference sample.

The variable $E_{511}/(1 + \nu)$ for the line (511) shown in Table 1 was calculated in the Royce approximation for crystals of cubic syngony [12]:

$$\frac{1+\nu}{E_{hkl}} = s_{11} - s_{12} - 3\Gamma\left(s_{11} - s_{12} - \frac{s_{44}}{2}\right),$$

$$\Gamma = \frac{h^2k^2 + k^2l^2 + l^2h^2}{(h^2 + k^2 + l^2)}.$$

The calculations were performed with the coefficients of elasticity c and flexibility s determined for AMg6 in [13] (Table 1).

It should be mentioned that in our case with the data from Table 1, the values of E and ν in the Royce and Voigt approximations do not differ in fact.

RESULTS AND DISCUSSION

One of the main distinctions of shock processing without coating from processing with coating is formation of a thin layer of molten material in the zone of laser treatment. As a consequence of interaction between the melt and active oxygen of surface plasma and water vapor, a film is generated on the material

Table 1. Coefficients of elasticity of the second order in AMg6 alloy

s_{11}, GPa^{-1}	s_{12}, GPa^{-1}	c_{44}, GPa	s_{44}, GPa^{-1}	μ, GPa	λ, GPa	$E_{511}/(1+\nu)$, GPa
14.2×10^{-3}	-4.81×10^{-3}	25.9	38.6×10^{-3}	25.9	52	52.4

surface containing up to 30–40 at % of oxygen according to elemental analysis. The appearance of the boundary of processed and unprocessed surface (the top and the bottom parts of the figure, respectively) is illustrated in Fig. 1a. The processed fragment of the surface at higher magnification is illustrated in Fig. 1b. The X-ray diffraction analysis does not reveal structurally ordered oxide phases, which can indicate both low extent of crystallinity of formed compounds and low thickness of oxide film.

Figure 2a illustrates fragments of X-ray patterns recorded at the surface of AMg6 samples before and after triple laser processing. The changes in the ratio of intensities of Al diffraction lines, which depends on processing multiplicity, are obvious. A similar result is achieved upon increase in the coefficient of overlapping. The change in the intensity of X-ray lines reflects existence of not only an oxide layer but also a surface recrystallized layer. Existence of the recrystallized layer is confirmed also by splitting of initial diffraction lines into two, one of which is displaced toward lower and the other toward higher angles (Fig. 2b). The displacement of lines toward higher or lower angles is due to the existence of tensile or compressive stresses in the layer, respectively.

The total thickness of the oxide and recrystallized layers (10–30 μm in our case) depends on the power density and processing multiplicity. Except for the surface layer, no noticeable distinctions between the microstructure of processed and unprocessed samples were revealed by either optical or scanning electron microscopy. The diffraction patterns of the samples after removal of the surface layer are characterized by the same features as upon processing with absorbing coating [10].

Laser shock processing leads to a significant (by 15–20% at a maximum) increase in microhardness $HV_{0.05}$ to the depth up to 1.5 mm. Figure 3 illustrates the microhardness in samples exposed to single and triple processing. One may mention the absence of an explicit dependence of $HV_{0.05}$ on processing multiplicity and a significant scatter of microhardness across the depth.

Since the main aim of laser shock processing in terms of engineering application is creation of the required level of residual compressive stresses in the material, for determination of the working interval of the radiation power density, the amplitude of plasma pressure occurring on the target surface was evaluated (Table 2). The calculations were carried out using the model in [14]. The maximum pressure P (GPa) created by the laser plasma in the regime of constraint of plasma cloud expansion by the water layer was determined as follows [15]:

$$P = 0.01\sqrt{\frac{\alpha}{\alpha + 3} Z I_0},$$

where α is the fraction of internal energy usually released in the form of heat energy, (typically $\alpha \approx 0.25$); I_0 (GW/cm^2) is the radiation power density on the material surface; and Z (g/(cm^2 s)) is the reduced shock impedance between the target and inertia medium (water) determined as follows:

$$\frac{2}{Z} = \frac{1}{Z_w} + \frac{1}{Z_t},$$
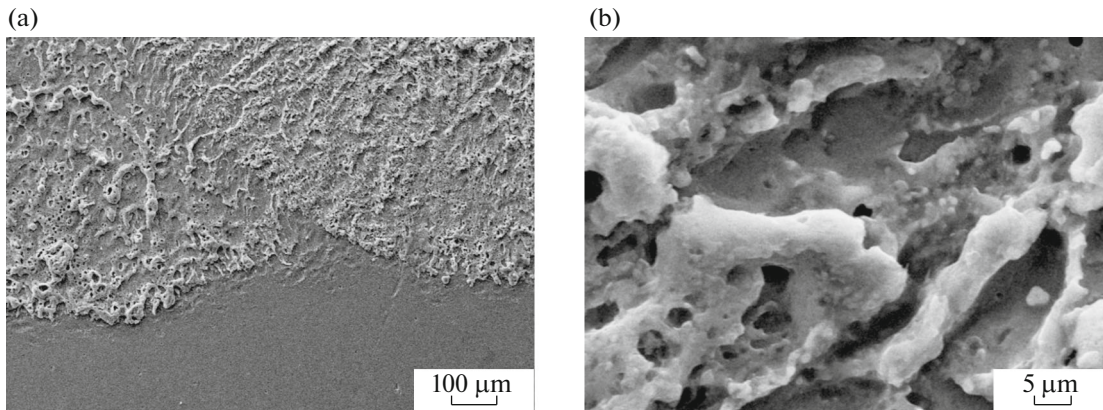
Fig. 1. Surface of AMg6 alloy without coating after laser shock processing.
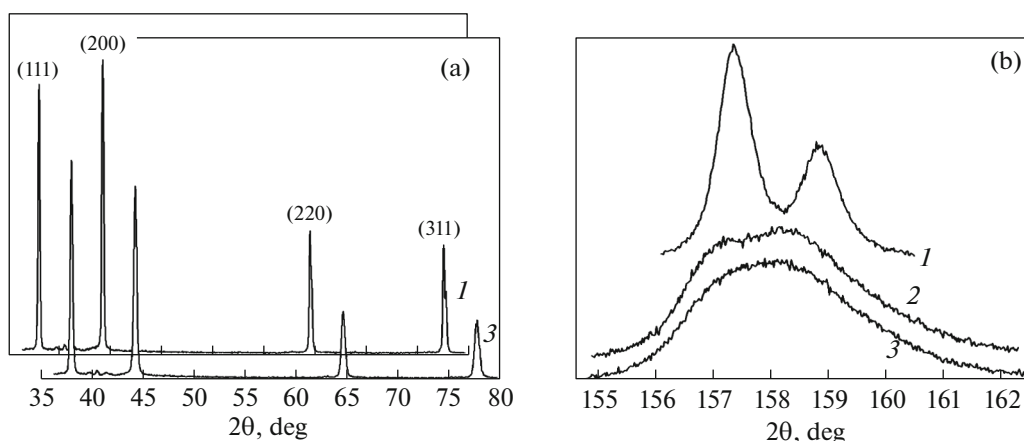
Fig. 2. X-ray diffraction patterns (a) and diffraction line (511) (b) of AMg6 alloy samples: (*1*) before laser processing; (*2*) single processing; (*3*) triple processing. $k_o = 0.65$; $q = 1.1$ GW/cm^2.

where Z_w and Z_t are the acoustic resistance of water and target, respectively.

In the entire used range of radiation power density, the plasma pressure formed on the target surface exceeded the Hugoniot elastic limit for AMg6 alloy ($\sigma_{HEL} = 0.42$ GPa). The Hugoniot elastic limit was determined by the well-known equation

$$\sigma_{HEL} = \left(1 + \frac{\lambda}{2\mu}\right)\sigma_{dyn},$$

where λ and μ are Lamé parameters (Table 1) and $\sigma_{dyn} = 210$ MPa is the dynamic yield compressive stress (the deformation rate is $1200-1300$ s^{-1}) [16]. The minimum radiation power density required for plasma pressure in excess of the Hugoniot elastic limit for AMg6 alloy should be at least 100 MW/cm^2. In the experiments, the compressive residual stresses on the material surface were recorded at $q \approx 200$ MW/cm^2, which quite satisfactorily agrees with the calculations.
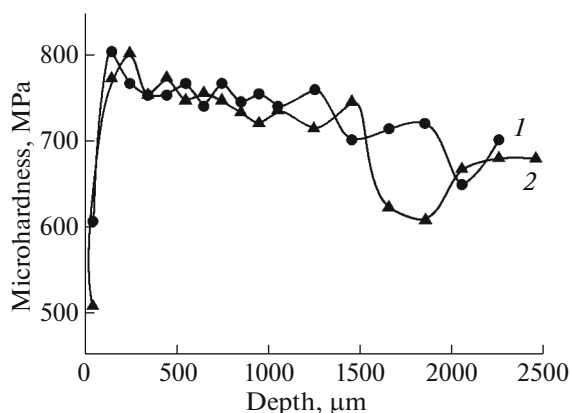
The distributions of residual stresses averaged along the directions x and y over depth in samples processed by radiation with different power density and $k_o = 0.5$ are illustrated in Fig. 4. As follows from the plots, the dependence of the stress profile on the power density is very complicated. Contrary to the processing with coating, the residual compressive stresses are characterized by an explicit maximum (σ_y up to -120 MPa) at the depth of ~100 μm, which is related to above-mentioned surface fusing, formation of oxide film, and, as a consequence, occurrence of tensile stresses in the surface layer.

In the range of $q = 0.7-2.2$ GW/cm^2 ($d = 1.4-2.5$ mm), the function $\sigma(h)$ has a wavelike pattern with minimum compressive stresses at the depth of $450-500$ μm and the depth of plastic deformation up to 1.6 mm. The increase in the coefficient of overlapping

Fig. 3. Microhardness of AMg6 alloy after single (*1*) and triple (*2*) processing. $k_o = 0.65$; $q = 1.1$ GW/cm^2.
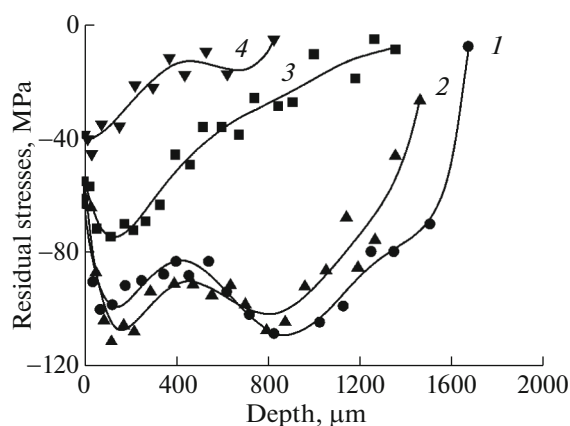

Fig. 4. Distribution of average residual stresses in processed samples at different power densities ($k_o = 0.5$): (*1*) 2.2; (*2*) 1.1; (*3*) 0.5; (*4*) 0.27 GW/cm^2.

Table 2. Calculated amplitudes of plasma pressures on AMg6 surface at different power densities of laser radiation

Z_t, g/(cm^2 s)	Z_w, g/(cm^2 s)	α	Z, g/(cm^2 s)	I_0, GW/cm^2	P, GPa
1.5×10^6	0.165×10^6	0.25	0.297×10^6	2.2	2.2
				1.1	1.6
				0.7	1.3
				0.5	1.1
				0.27	0.8

leads to a significant increase in the depth of the region of plastic deformation (Fig. 4, plot *2* and Fig. 5, plot *1*).

Significant influence on formation of residual stresses is exerted by the existence of the cladding aluminum layer on the material surface. In fact, it acts as a protective coating and, being the material for generation of plasma cloud, at the same time protects the main material against thermal exposure. Laser shock processing in the presence of such layer leads to a significant difference in residual stresses along (σ_x) and across (σ_y) passes, as well as to a significant increase in their maximum value on the surface of the main material in comparison with processing of alloy without cladding layer (Figs. 6a and 5, respectively). In addition, a noticeable difference should be mentioned in the results of processing of samples with cladding aluminum layer and samples with coating in the form of adhesive polymer tape described in [10]. At a lower number of pulses per unit surface area (155 and 175 pulse/cm^2, respectively) and half the power density, the depth of the zone of plastic deformation and the residual compressive stresses in cladded samples are significantly higher (Fig. 6). Obviously, this is a consequence of different conditions of formation and propagation of shock wave due to different properties

of coating materials and contact areas water–coating and coating–AMg6 alloy.

The increase in multiplicity of processing influences comparative weakly the maximum residual stresses, slightly varying their profile (Fig. 5) and increasing the depth of formation of negative stresses up to 40%. In the case of alteration of processing direction in each cycle, the multiplicity influences the ratio of σ_x and σ_y. If upon single processing σ_y/σ_x varies mainly in the range of 1–1.2 and upon double processing $\sigma_x \approx \sigma_y$, then triple processing results in $\sigma_y/\sigma_x = 0.8$–0.9.

When analyzing in detail the profile of residual stresses (Figs. 4–6), one can see that, at the depth from 500 to 1500 μm, their distribution has wavelike pattern with regard to the approximating curve. Since the formation of residual stresses due to the absence of phase peening in the considered case is mainly related to the dislocation structure, it is possible to assume that such distribution is dictated by layer-by-layer variation of the dislocation density over the depth.

The dislocation density and other structural properties were determined by analysis of the profile of X-ray diffraction line (200), since in FCC lattices the structural defects are best of all exposed in variation of the profile of this line. With this aim, experimental and instrumentation lines were approximated by asymmetric pseudo-Voigt functions. The apparent size of coherent scattering regions (CSR) D and the value of microdeformation ε, as in [10], were calculated by the analytical results in [17]. The equations in [17] make it possible to calculate D and ε with consideration for asymmetry of instrumentation and physical lines without performing deconvolution for recovery of the physical profile. The dislocation density was calculated by the equation used in analysis of plastically deformed FCC metals [18]:

$$\rho = \frac{2\sqrt{3}\varepsilon}{bD},$$

where $b = a/\sqrt{2}$ is the modulus of the Burgers vector and a is the unit cell parameter.

According to the calculations, on the surface of unprocessed material, $D = 120$–160 nm, $\varepsilon = 0.0007$–0.0008, and dislocation density $\rho = 6.2 \times 10^{13}$–7 × 10^{13} m^{-2}. The structural properties of unprocessed
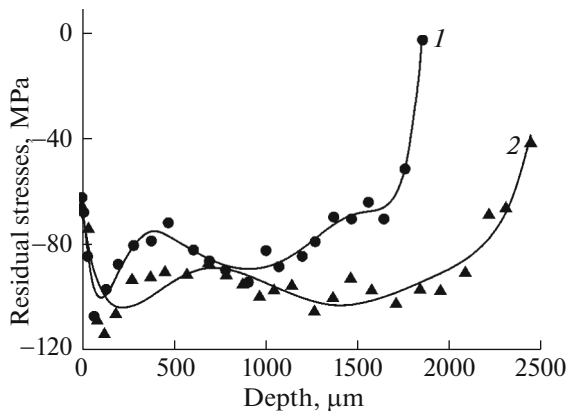

Fig. 5. Distribution of the measured average residual stresses in samples with different multiplicity of processing ($k_0 = 0.65$, $q = 1.1$ GW/cm^2): (*1*) single processing; (*2*) triple processing.
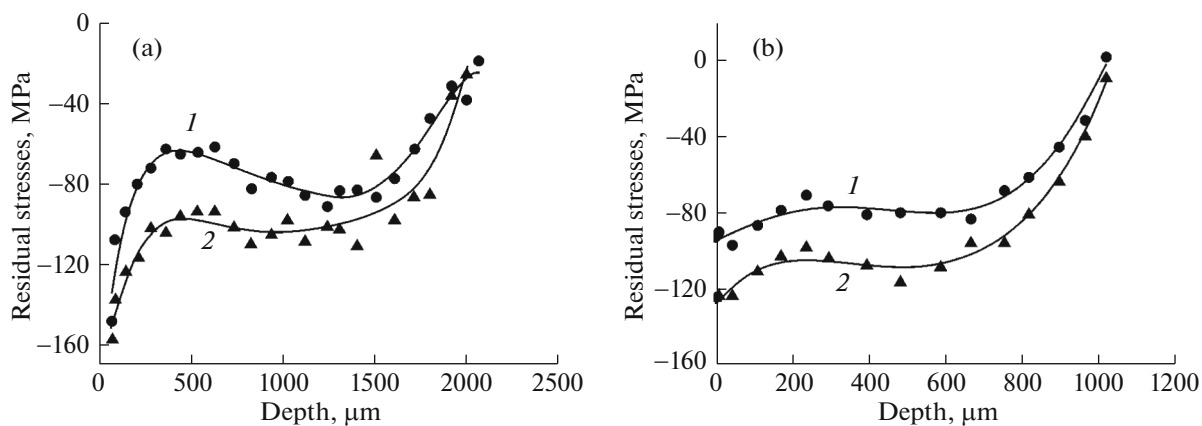
Fig. 6. Distribution of measured average residual stresses σ_x and σ_y in processed samples with coating: (a) cladding Al layer, $q = 1.1$ GW/cm^2; (b) polymer coating, $q = 2.2$ GW/cm^2.
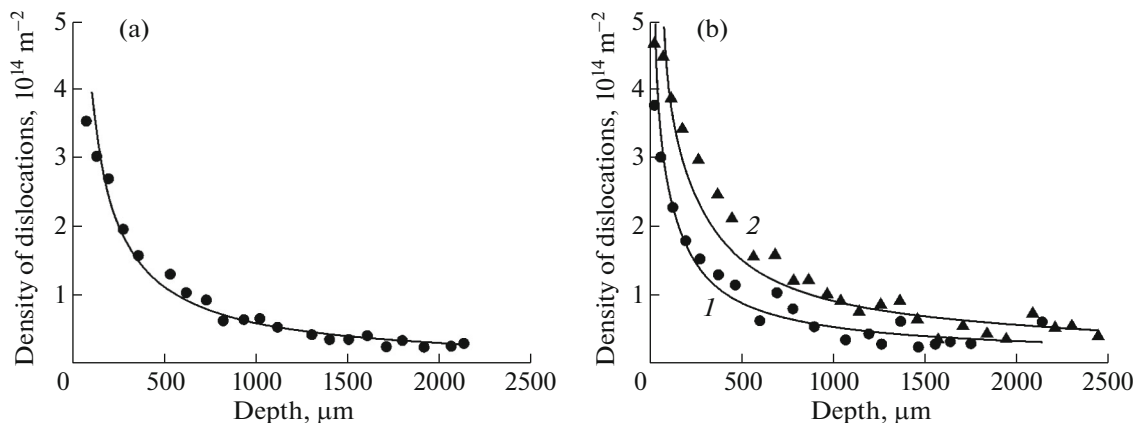

Fig. 7. Dependences of the average density of dislocations on the depth in processed samples with cladding layer (a) and with different multiplicity of processing (b): (*1*) single processing; (*2*) triple processing. $k_o = 0.65$, $q = 1.1$ GW/cm^2.

samples are characterized by an obvious dependence on radiation power density and multiplicity of processing. Thus, the minimum $D \approx 50$ nm, the maximum $\varepsilon \approx 0.0019$, and the maximum dislocation density $\rho \approx 4.7 \times 10^{14}$ m^{-2} are achieved on the surface (after etching of the oxidized layer) in the course of triple processing. Figure 7 illustrates the dislocation densities as a function of depth for samples processed under different conditions (corresponding to the samples in Fig. 5 and Fig. 6a). In the course of single processing of AMg6 with cladding layer, the changes in dislocation density can be described using the following equation: $\rho(h) = bx^{-a}$, where $a = 0.94$. For samples without cladding layer, the dislocation density as a function of depth has a more complicated form. The wavelike pattern of the dislocation density distribution with regard to the approximating curve at the depth of 450−2000 μm should be mentioned, which correlates quite well with the distribution of corresponding resid-

ual compressive stresses. In Figs. 7a and 7b, it is possible to determine sufficiently precisely the depth of plastic deformation upon laser treatment, which also correlates satisfactorily with the microhardness as a function of depth. The scatter of microhardness values across the depth can be attributed to generation of layers with different crystallographic properties after shock processing. In this case, in contrast to the microhardness, X-ray structural analysis makes it possible to determine more precisely the depth of the processing zone (the zone of plastic deformation) during laser shock processing.

The observed features of the distribution of dislocations and profiles of residual compressive stresses, in addition to the parameters of laser processing, can be attributed to the formation of a surface recrystallized layer, the specificity of formation of shock waves in the presence of a water layer of high thickness, and the influence of waves reflected from rear side of sam-

ples on the material structure, which form significant tensile stresses. However, supplemental studies are required to account for the contribution of these factors.

CONCLUSIONS

This work demonstrated the efficiency of laser shock processing of AMg6 aluminum alloy without absorbing coating for creation of residual compressive stresses to the depth up to 2 mm. The profile of residual stresses was determined as a function of the power density of laser pulse, and its boundary value was determined, equal to 200 MW/cm^2, at which residual stresses can be formed.

X-ray structural analysis demonstrated an explicitly pronounced correlation between dislocation density and residual stresses over the depth of laser treatment area. With increase in the power density of laser radiation and multiplicity of processing, the average dislocation density on the material surface increases to 4.7×10^{14} m^{-2}, the sizes of coherent scattering regions decrease to 50 nm, and the value of microstrains increases to 0.0019.

Increase in the multiplicity of processing influences the ratio σ_x/σ_y and increases the depth of formation of residual stresses by 1.3—1.4 times, weakly influencing their maximum value.

The existence of cladding aluminum layer leads to increase in the maximum value of residual compressive stresses from −120 to −155 MPa and changes in the distribution of dislocation density over the depth in comparison with processing of alloy without cladding layer or with protective polymer coating.

REFERENCES

1. Gujba, A.R. and Medraj, M., Laser peening process and its impact on materials properties in comparison with shot peening and ultrasonic impact peening, *Materials*, 2014, vol. 7, pp. 7925–7974.

2. Chupakhin, S., Klusemann, B., Huber, N., and Kashaev, N., Application of design of experiments for laser shock peening process optimization, *Int. J. Adv. Manuf. Technol.*, 2019, vol. 102, nos. 5–8, pp. 1567–1581.

3. Sundar, R., Ganesh, P., Gupta, R.K., Ragvendra, G., Pant, B.K., Kain, V., Ranganathan, K., Kaul, R., and Bindra, K.S., Laser shock peening and its applications: A review, *Lasers Manuf. Mater. Process.*, 2019, vol. 6, pp. 424–463.

4. Wu, J., Zhao, J., Qiao, H., Hu, X., and Yang, Y., The new technologies developed from laser shock processing, *Materials,* 2020, vol. 13, no. 6, art. ID 1453. https://doi.org/10.3390/ma13061453

5. Liao, Y., Ye, C., and Cheng, G.J., A review: Warm laser shock peening and related laser, *Opt. Laser Technol.*, 2016, vol. 78, part A, pp. 15–24.

6. Prabhakaran, S. and Kalainathan, S., Warm laser shock peening without coating induced phase transformations and pinning effect on fatigue life of low-alloy steel, *Mater. Des.*, 2016, vol. 107, pp. 98–107.

7. Sano, Y., Akita, K., Masaki, K., Ochi, Y., Altenberger, I., and Scholtes, B., Laser peening without coating as a surface enhancement technology, *J. Laser Micro/Nanoeng.*, 2006, vol. 1, no. 3, pp. 161–166.

8. Karthik, D. and Swaroop, S., Laser peening without coating—an advanced surface treatment: A review, *Mater. Manuf. Process.*, 2016, vol. 32, pp. 1565–1572.

9. Zhu, J., Jiao, X., Zhou, C., and Gao, H., Applications of underwater laser peening in nuclear power plant maintenance, *Energy Procedia*, 2012, vol. 16, part A, pp. 153–158.

10. Bakulin, I.A., Kakovkina, N.G., Kuznetsov, S.I., Panin, A.S., and Tarasova, E.Yu., Structure and residual stresses in the AMg6 alloy after laser shock processing, *Inorg. Mater.: Appl. Res.*, 2021, vol. 12, pp. 55–60. https://doi.org/10.1134/S2075113321010032

11. Komyak, N.I. and Myasnikov, Yu.G., *Rentgenovskie metody i apparatura dlya opredeleniya napryazhenii* (X-Ray Methods and Equipment for Determining Stresses), Leningrad: Mashinostroenie, 1972.

12. Singh, A.K. and Balasingh, C., Analysis of lattice strains measured under non-hydrostatic pressure, *J. Appl. Phys.*, 1998, vol. 83, no. 12, pp. 7567–7575.

13. Volkov, A.D., Kokshaiskii, A.I., Korobov, A.I., and Prokhorov, V.M., Second- and third-order elastic coefficients in polycrystalline aluminum alloy AMg6, *Acoust. Phys.*, 2015, vol. 61, no. 6, pp. 651–656.

14. Berthe, L., Fabbro, R., Peyre, P., Tollier, L., and Bartnicki, E., Shock waves from a water-confined laser-generated plasma, *J. Appl. Phys.*, 1997, vol. 82, no. 6, pp. 2826–2832.

15. Fabbro, R., Fournier, J., Ballard, P., Devaux, D., and Virmont, J., Physical study of laser produced plasma in confined geometry, *J. Appl. Phys.,* 1990, vol. 68, no. 2, pp. 775–784.

16. Glushak, B.L., Ignatova, O.N., Pushkov, V.A., Novikov, S.A., Girin, A.S., and Sinitsyn, V.A., Dynamic deformation of aluminum alloy AMg-6 at normal and higher temperatures, *J. Appl. Mech. Tech. Phys.*, 2000, vol. 41, no. 6, pp. 1083–1086.

17. Pantoja-Cortes, J., Sanchez-Bajo, F., and Ortiz, A.L., A line-broadening analysis model for the microstructural characterization of nanocrystalline materials from asymmetric X-ray diffraction peaks, *J. Phys.: Condens. Matter*, 2012, vol. 24, no. 21, art. ID 215301. https://doi.org/10.1088/0953-8984/24/21/215301

18. Ortiz, A.L., Tian, J.W., Villegas, J.C., Shaw, L.L., and Liaw, P.K., Interrogation of the microstructure and residual stress of nickel-base alloy subjected to surface severe plastic deformation, *Acta Mater.,* 2008, vol. 56, pp. 413–426.

Translated by I. Moshkin